



Contents lists available at ScienceDirect



CFD modeling a fluidized bed large scale reactor with various internal elements near the heated particles feeder

Olga V. Soloveva^{a,b}, Sergei A. Solovev^{c,d,*}, Svetlana R. Egorova^b, Alexander A. Lamberov^b, Alexey V. Antipin^d, Emil V. Shamsutdinov^a

^a Institute of Heat Power Engineering, Kazan State Power Engineering University, Krasnoselskaya St. 51, 420066 Kazan, Russia

^b Institute of Chemistry, Kazan Federal University, Kremlevskaya St. 29, 420111 Kazan, Russia

^c Institute of Mechanics and Engineering — Subdivision of the Federal State Budgetary Institution of Science “Kazan Scientific Center of the Russian Academy of Science”, Lobachevskiy St. 2/31, 420111 Kazan, Russia

^d Institute of Mathematics and Mechanics, Kazan Federal University, Kremlevskaya St. 35, 420008 Kazan, Russia

ARTICLE INFO

Article history:

Received 7 December 2017

Received in revised form 1 August 2018

Accepted 7 August 2018

Available online 28 August 2018

Keywords:

Fluidized bed

Gas-solid flow

Computational fluid dynamics

Internal elements

Particle feeder

Fine particles

Heating

ABSTRACT

A numerical study of the fluidized bed industrial reactor in the presence of various internal elements is carried out by CFD methods. A simple reactor heating efficiency function of chemical reaction with heat absorption is considered. The main emphasis is placed on the circulation flows of the catalyst particles and heating of the reactor. The analysis of the impact of various design elements on the heating efficiency of the reactor is carried out. Particular attention is paid to the possibility of baffles applying, which allows redirecting the flow. This effect may have an especially important value when the rapid heating of the reactor is required for temperature dependent reactions. The influence of heated catalyst feeder design on the efficiency of whole reactor heating is studied. The influence of the fractional composition of the catalyst, namely the presence of fine particles, on the reactor heating efficiency for different reactor design features is also studied. The results are carried out for a specific reactor example, but contribute to the overall branch of fluidized bed engineering.

© 2018 Institution of Chemical Engineers. Published by Elsevier B.V. All rights reserved.

1. Introduction

Fluidized bed gas-solid reactors are widely used in the chemical and petroleum industry and gasification of coal and biomass (Kunii and Levenspiel, 1991; Grace et al., 1997; Yang, 2003; Basu, 2006; Sadeghbeigi, 2012) due to the high efficiency of heat and mass transfer between the components. Even though such an apparatus has been used in industry for more than fifty years there is still a high demand in the study of fluidized bed properties and applications.

The investigations on laboratory fluidized bed apparatus do not provide complete results for industrial large-scale reactors. Currently one of the most reliable methods of determining the properties of the

large-scale fluidized beds is a tomographic scanning, as presented by the recent works (Chen et al., 1999; Jin et al., 2005; Patel et al., 2008; Heindel et al., 2008; Wang et al., 2012; Mandal et al., 2012; Escudero and Heindel, 2014; Kingston et al., 2015).

One of the possible ways to get the data is a numerical simulation. Computational fluid dynamics (CFD) is a very effective tool for understanding fluidized bed hydrodynamics including heat and mass transfer. CFD is important in optimization and design of industrial large-scale reactors. Solving equations numerically allows carrying out calculations of different possible mechanisms of the fluidization process, both in terms of basic research and practical application. Numerical calculations of fluidization are usually based on

* Corresponding author at: Institute of Mathematics and Mechanics, Kazan Federal University, Kremlevskaya St. 35, 420008 Kazan, Russia.

E-mail address: serguei.s349@mail.ru (S.A. Solovev).

<https://doi.org/10.1016/j.cherd.2018.08.011>

0263-8762/© 2018 Institution of Chemical Engineers. Published by Elsevier B.V. All rights reserved.

Nomenclature

A	interfacial area (m^2)
C_{ef}	reactor heating efficiency coefficient (-)
C_D	drag coefficient (-)
d	diameter (m)
e	coefficient of restitution (-)
F_{ef}	reactor heating efficiency function (K)
g	gravitational acceleration (m s^{-2})
g_0	radial distribution coefficient (-)
h	enthalpy (J)
I	unit tensor (-)
K	interphase exchange coefficient (kg s^{-1})
k	diffusion coefficient for granular energy (-)
N_C	Courant number (-)
Nu	Nusselt number (-)
p	pressure (Pa)
Pr	Prandtl number (-)
Q	intensity of heat exchange (W)
R	interphase exchange force (N)
Re	Reynolds number (-)
t	time (s)
T	temperature (K)
v	velocity (m s^{-1})

Greek letters

α	volume fraction (-)
ϕ	energy exchange ($\text{kg m}^{-1}\text{s}^{-3}$)
γ	collisional dissipation of energy ($\text{kg m}^{-1}\text{s}^{-3}$)
κ	thermal conductivity (W K^{-1})
λ	bulk viscosity ($\text{kg m}^{-1}\text{s}^{-1}$)
μ	shear viscosity ($\text{kg m}^{-1}\text{s}^{-1}$)
Θ	granular temperature (m^2s^{-2})
ρ	real density (kg m^{-3})
τ	stress tensor (Pa)

Subscripts

g	gas phase
s	solid phase

Eulerian–Lagrangian and Eulerian–Eulerian approach. The solid phase is considered as discrete particles in Eulerian–Lagrangian approach (e.g. Chen and Wang, 2014; Zhou, Q. et al., 2016). In this approximation, each particle is treated separately. It requires considerable computing resources and is laborious for industrial devices that work with a hundred tons of particles. In Eulerian–Eulerian approach, the carrier (gas, liquid) and the discrete (solid) phase are considered as continuous. To account for the particle interaction in the fluidized bed, by analogy with the kinetic theory of gases, we added an equation describing the change in the kinetic energy of particles due to their collision (e.g., Gidaspow, 1994). This approach is less demanding in terms of computational resources. However, there is a problem of creating reliable models of interaction between phases and boundaries. The development of such models continues to this day. There are different mathematical models for resistance forces, viscosity, heat transfer, etc., and their parameters are studied for possible applications by means of numerical simulations (Chalermisinsuwan et al., 2012; Peng et al., 2013; Shuai et al., 2015; Upadhyay and Park, 2015). Some papers are focused on the effect of wall boundary condition in CFD modeling of fluidized bed hydrodynamics (Zhong et al., 2012; Li and Benyahia, 2013; Loha et al., 2013; Bakshi et al., 2015; Gupta et al., 2016; Fede et al., 2016).

Particle size distribution plays an important role in the behavior of fluidized bed. Adding fine particles (diameter $<45 \mu\text{m}$, Yates and Newton, 1986) reduces the bubble sizes and increases the reaction rates.

In some cases, the addition of fine particles leads to a bed expansion and an increase in the dense phase porosity (Yates and Newton, 1986; Kono et al., 1987; Grace and Sun, 1991; van Ommen et al., 2007). However, in other cases, the addition of these particles leads to a reduction of the solid phase porosity (Khoe et al., 1991; Saayman et al., 2013). The possibility of reducing the effective viscosity in the fluidized bed substantially by adding fine particles was experimentally demonstrated in Kono et al. (1986). Authors (Beetstra et al., 2009) showed that the addition of fine particles only slightly reduces the effective viscosity. Experimental results showing the reduction in the bubble sizes by fast X-ray tomography were obtained in Brouwer et al. (2012). The influence of fine particles on fluidization was investigated in Gu et al. (2016) by numerical simulations. It was shown that the addition of a large number of fine particles suppresses the bubbles and the apparatus can reach a stable solid-like operating regime.

Each element of the chemical fluidized bed reactor can have a significant impact on hydrodynamics, processes of heat and mass transfer, and the overall efficiency of the apparatus. For example, obviously, the shape of the gas feeder will affect the particle motion. The results of calculations for a bed in a rectangular chamber with various forms of nozzles and their effect on the motion of the particles are presented in Deb and Tafti (2014). Modeling and comparative analysis of two large fluidized bed units with various gas feeders were carried out in Solov'ev et al. (2016). The influence of the gas feeder on the variation of the circulation flows and the efficiency of industrial reactors is shown here. The location of internal elements in the fluidized bed reactor may affect the operation of the apparatus. Experimental studies of internal elements in a liquid–solid fluidized bed are presented in Piovano et al. (2015). The significant decrease in the bed expansion for a given liquid superficial velocity is shown in this paper. The tapered circulating fluidized bed reactor risers are studied in Chalermisinsuwan et al. (2009, 2010). The criteria of geometry type for different reaction characteristics are shown there as well. Effect of bed geometry on the hydrodynamics of slot-rectangular spouted beds was studied in Golshan et al. (2017).

A downward movement of the solid particles along the walls with a high particle concentration is observed in fluidization in cylindrical columns. This effect ensures continuous circulation of the particles in the apparatus. The near wall dense ring in a large-scale down-flow circulating fluidized bed is investigated experimentally in Zhang et al. (2003). Particle motion near the walls is researched in Wang and Rhodes (2005) by discrete element method. One main problem is to ensure a satisfactory contact between the gas and solid particles. The bubbles in the fluidized bed have a negative effect on the processes of heat and mass transfer. The bubble's breakage in fluidized bed is studied experimentally in Movahedirad et al. (2014). The effects of the reduction of the fluidization column diameter on the fluidization quality are considered in Ansart et al. (2017).

Some papers present the attempts to control the fluidized bed flow by using structural elements, where researches focus on the baffles. Such structures allow to redirect a near wall particles flow and to change the general circulation flows in the apparatus. Authors of the paper (Jiang et al., 1991) researched internal ring baffles that improve the chemical reaction efficiency by increasing the particle concentration in the radial direction. Influence of ring-type internals on axial pressure distribution is experimentally investigated in Bu and Zhu (1999). The changes in the character of the movement and particle concentration along the wall with deflectors are shown in Golriz and Grace (2002). Thesis elements increase the heat transfer between the suspension and the wall. The papers (Samruamphiansun et al., 2012; Chalermisinsuwan et al., 2014) focus on the experimental and numerical study of the effect of the ring baffles on the hydrodynamics of the fluidized bed. The considered elements are used for improving the mixing and heat and mass transfers in the system. Authors of papers (Guio-Perez et al., 2013, 2014) concluded that ring-type internals capable to optimize fluidized bed system for process requirements by gas and particle residence time control. Experimental and numerical investigations of the apparatus with perforated plates and louver baffles are presented in Yang et al. (2015, 2016). Numerical gas–solid flow analysis of ring-baffled risers is carried out in Rossbach et al. (2016).

Investigations of the particle distribution and kinetic energy and turbulent energy dissipation rate are studied there as well. In the paper Zhou, E. et al. (2016), a pronation-grille baffle was designed and used to improve the fluidization quality of gas–solid dense phase fluidized bed.

In the current paper, a mathematical model is constructed and applied to the operation of an industrial fluidized bed reactor using numerical simulation. The reactor works with a pulverized catalyst and is designed to dehydrogenate isobutane to isobutylene at the temperature of 550–650 °C. We consider that the fluidized bed reactor of cylindrical shape with internal structural elements which are the cheapest methods for bubbles breaking and flow control. The ring baffles, deflectors and the grids were investigated as the internal components. The grids provide the breaking of the rising bubbles. The ring baffles and deflectors provide the deviation in the solid particle flow. The main aim of the present paper is to determine the influence of the internal elements on the circulation flow of gas and particles and whole reactor heating and efficiency. The hydrodynamic and thermal characteristic operating parameters, such as the field of particle concentration and the temperature of the gas, were obtained by the numerical calculations. The effect of internal elements on the behavior of the catalyst in the reactor and the reactor heating efficiency were investigated.

2. Problem formulation and CFD model

2.1. The large-scale industrial reactor

The work is based on mathematical modeling of hydrodynamics and heat transfer processes in the industrial chemical fluidized bed reactor designed for the isobutane dehydrogenation. The reactor column has a height of 11 m and 5.2 m in diameter in the active zone. A gas–raw feeder is located in the lower part of the reactor; the reactor's load is 20–40 tons per hour of raw material gas flow rate. The gas is supplied at a temperature of 550 °C. In the active zone of the reactor, there is a chromia-alumia microspheroidal catalyst with the particle diameter of 20–200 μm. A vertical supply pipe from the regenerator of the heated fresh catalyst is located in the center of the reactor. The average catalyst feed rate to the reactor is 60–100 tons per hour. Catalyst from the regenerator is supplied at the temperature of 650 °C. The pipe extends from the bottom of the reactor to a height of 7 m and is 0.3 m in diameter. There is a channel for the waste catalyst removed into the regenerator at the bottom of the reactor. From the principle of maintaining a balance, the waste catalyst is taken in the volume of incoming fresh catalyst. Ten rows of grids of the angular type with a free-sectional area of about 30% are located in the middle of the reactor in the working zone (grid sizes are presented in Fig. 1). Grids and baffles have an influence on voidage and particle residence time in fluidized bed reactor (Klenov et al., 2017). A pronation-grille baffle can effectively destroy bubbles and improve the axial and radial distribution of the bed density (Zhou, E. et al., 2016). Six pairs of the cyclones are placed in the upper part of the reactor to separate the gas leaving the reactor and return the catalyst particles into the working zone of the reactor.

It is required to determine the hydrodynamic and thermal characteristics of the processes taking place in the reactor. Main attention is paid to the influence of structural elements, in particular grids, baffles, and gas and catalyst feeders, to the efficiency of reactor heating. It is necessary to carry out an upgrade of the reactor's design to increase the reactor product yield.

2.2. Reactor model

The chemical reactor considered consists of various elements and has a macro and microelements. The construction of a complete 3D model based on all structural features of the geometry would lead to very high costs of computer capacity and computational time. As the analyzed reactor has a cylindrical structure, its model for calculations was constructed assuming the axial symmetry. It is assumed that an arbitrary vertical cross-section of the reactor completely characterizes the processes taking place in the reactor. Fig. 1 shows the geometry used in the calculations.

The axial symmetry model suggests that the problem solved is not plane 2D and the reactor model is constructed by rotating the geometry shown in the figure around its symmetry axis. The geometric dimensions of the model correspond to the geometric dimensions of the analyzed reactor.

2.3. Fluidized bed mathematical model

The numerical simulation of the fluidized bed in a chemical reactor was performed using a continuous multiphase Euler–Euler model complemented with the kinetic theory of gases to include the collisions between solid particles. Equations are presented in Tables 1 and 2.

This equations system is unclosed. To close it we use the relations obtained from the experimental studies of the fluidized bed.

The gas motion considered in the reactor at the accepted loads of the raw gas feeding and parameters of the catalyst used is turbulent. In the model accepted for the calculations a dispersed $k - \varepsilon$ model of turbulence was used in which the motion of the “secondary” solid granular phases is generated on the background of the turbulent motion of the “primary” gas phase.

Differential equations that describe the hydrodynamic and thermal processes in the computational field of the reactor's model were solved in CFD ANSYS Fluent 14.5 for the scheme of unsteady flow. Fluidization modeling is also used in other CFD codes (e.g. Marschall et al., 2011; Liu and Hinrichsen, 2014a; Liu and Hinrichsen, 2014b; Gu et al., 2016).

2.4. Particle size

A large industrial reactor operates at high temperature and has thick insulating walls; hence it is not possible to evaluate the particle motion visually and make a comparison with the results of numerical simulation. Laboratory experiments on small tubes have significant differences from the large industrial reactors, but allow us to choose approximations for the calculations. For example, we can estimate the average particle size and the effect fine particles have on the average volume fraction of the solid phase and the fluidized bed height.

As mentioned before, catalyst particles in the reactor have a wide range of sizes. But using the whole fractional composition in calculations is too expensive, this is why we select the particle size for calculations. The calculated Sauter mean diameter is about 100 μm. For the analysis of the adequacy of this particle size, laboratory experiments were carried out on a transparent glass tube with a diameter of 2.2 cm and height of 1 m, with uniform airflow feed. Before entering the tube air stream passes through the container with hot water to reduce the occurrence of electrostatic charge (Movahedirad

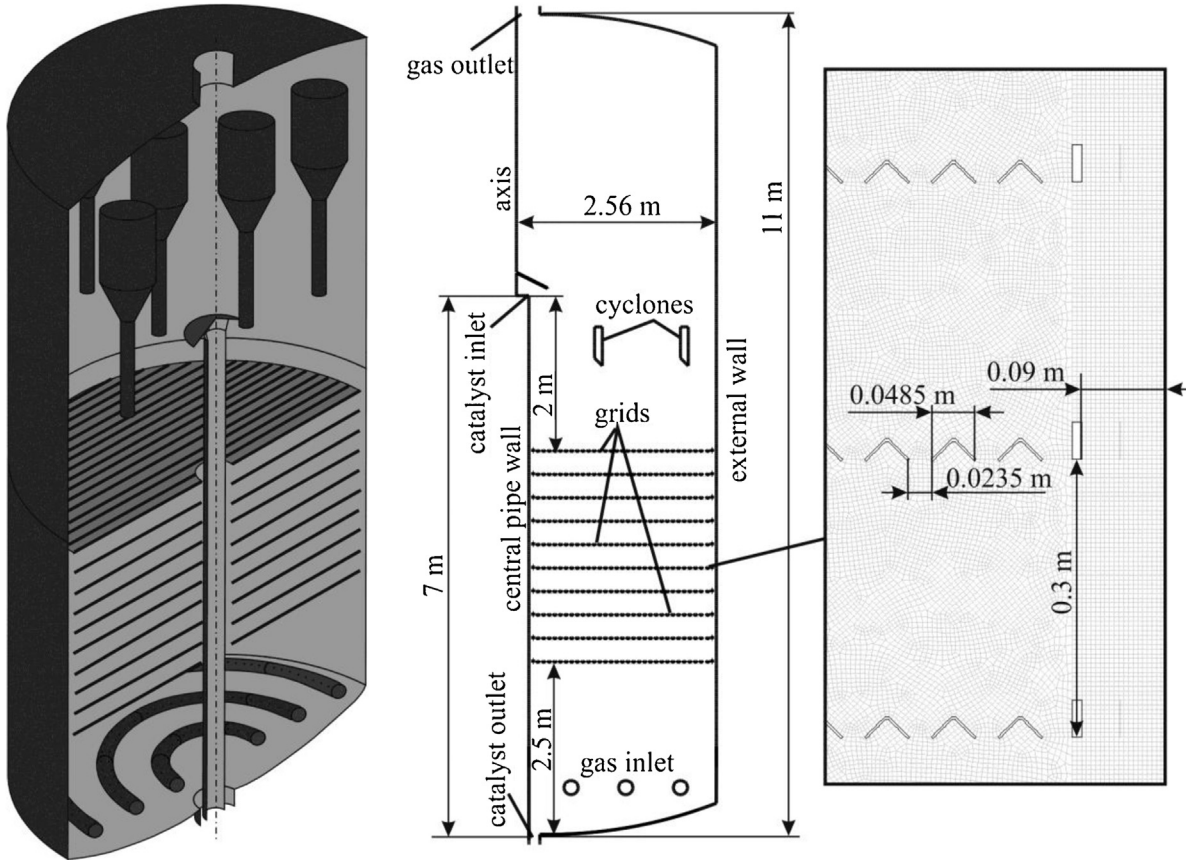


Fig. 1 – The reactor model scheme.

Table 1 – The conservation equations.

Conservation of mass for the gas phase

$$\frac{\partial \alpha_g \rho_g}{\partial t} + \nabla \cdot (\alpha_g \rho_g \vec{v}_g) = 0 \quad (1)$$

Conservation of mass for the i-th solid particle phase

$$\frac{\partial \alpha_{s,i} \rho_{s,i}}{\partial t} + \nabla \cdot (\alpha_{s,i} \rho_{s,i} \vec{v}_{s,i}) = 0 \quad (2)$$

Conservation of momentum for the gas phase

$$\frac{\partial \alpha_g \rho_g \vec{v}_g}{\partial t} + \nabla \cdot (\alpha_g \rho_g \vec{v}_g \vec{v}_g) = -\alpha_g \nabla p + \nabla \cdot \tilde{\tau}_g + \alpha_g \rho_g \vec{g} + \sum_{i=1}^N K_{gs,i} (\vec{v}_g - \vec{v}_{s,i}) \quad (3)$$

Stress for the gas phase

$$\tilde{\tau}_g = \alpha_g \mu_g (\nabla \vec{v}_g + \nabla \vec{v}_g^T) + \alpha_g \frac{2}{3} \mu_g \nabla \cdot \vec{v}_g \tilde{I} \quad (4)$$

Conservation of momentum for the i-th solid particle phase

$$\begin{aligned} \frac{\partial \alpha_{s,i} \rho_{s,i} \vec{v}_{s,i}}{\partial t} + \nabla \cdot (\alpha_{s,i} \rho_{s,i} \vec{v}_{s,i} \vec{v}_{s,i}) &= -\alpha_{s,i} \nabla p - \nabla p_{s,i} + \nabla \cdot \tilde{\tau}_{s,i} + \\ &+ \alpha_{s,i} \rho_{s,i} \vec{g} + K_{s,ig} (\vec{v}_{s,i} - \vec{v}_g) + \sum_{j=1}^{N-1} K_{s,is,j} (\vec{v}_{s,i} - \vec{v}_{s,j}) \end{aligned} \quad (5)$$

Stress for the solid particle phase

$$\tilde{\tau}_{s,i} = \alpha_{s,i} \mu_{s,i} (\nabla \vec{v}_{s,i} + \nabla \vec{v}_{s,i}^T) + \alpha_{s,i} \left(\lambda_{s,i} - \frac{2}{3} \mu_{s,i} \right) \nabla \cdot \vec{v}_{s,i} \tilde{I} \quad (6)$$

Conservation of solid particle phase fluctuating energy (Ding and Gidaspow, 1990)

$$\begin{aligned} \frac{3}{2} \left[\frac{\partial}{\partial t} (\alpha_{s,i} \rho_{s,i} \Theta_{s,i}) + \nabla \cdot (\alpha_{s,i} \rho_{s,i} \vec{v}_{s,i} \Theta_{s,i}) \right] &= \\ (-p_{s,i} \tilde{\tau}_{s,i} + \tilde{\tau}_{s,i}) : \nabla \vec{v}_{s,i} + \nabla \cdot (k_{\Theta_{s,i}} \nabla \Theta_{s,i}) - \gamma_{\Theta_{s,i}} + \phi_{g,s,i} + \sum_{j=1}^{N-1} \phi_{s,j,s,i} & \end{aligned} \quad (7)$$

Conservation of energy for the gas phase

$$\frac{\partial \alpha_g \rho_g h_g}{\partial t} + \nabla \cdot (\alpha_g \rho_g \vec{v}_g h_g) = \alpha_g \frac{\partial p_g}{\partial t} + \tilde{\tau}_g : \vec{v}_g + \sum_{i=1}^N h_{gs,i} A (T_g - T_{s,i}) \quad (8)$$

Conservation of energy for the i-th solid particle phase

$$\frac{\partial \alpha_{s,i} \rho_{s,i} h_{s,i}}{\partial t} + \nabla \cdot (\alpha_{s,i} \rho_{s,i} \vec{v}_{s,i} h_{s,i}) = \alpha_{s,i} \frac{\partial p_{s,i}}{\partial t} + \tilde{\tau}_{s,i} : \vec{v}_{s,i} + h_{s,ig} A (T_{s,i} - T_g) + \sum_{j=1}^{N-1} h_{s,is,j} A (T_{s,i} - T_{s,j}) \quad (9)$$

Table 2 – Constitutive equations.

Shear viscosity for the solid particle phase (Gidaspow, 1994)

$$\mu_{s,i} = \frac{4}{5} \alpha_{s,i} \rho_{s,i} d_{s,i} g_{0,s,i,s,i} (1 + e_{s,i,s,i}) \left(\frac{\Theta_{s,i}}{\pi} \right)^{\frac{1}{2}} + \frac{\alpha_{s,i} \rho_{s,i} d_{s,i} \sqrt{\Theta_{s,i} \pi}}{6(3 - e_{s,i,s,i})} \left[1 + \frac{2}{5} (1 + e_{s,i,s,i}) (3e_{s,i,s,i} - 1) \alpha_{s,i} g_{0,s,i,s,i} \right] \quad (10)$$

Bulk viscosity for the solid particle phase (Lun et al., 1984)

$$\lambda_{s,i} = \frac{4}{3} \alpha_{s,i}^2 \rho_{s,i} d_{s,i} g_{0,s,i,s,i} (1 + e_{s,i,s,i}) \left(\frac{\Theta_{s,i}}{\pi} \right)^{\frac{1}{2}} \quad (11)$$

Pressure for the solid particle phase

$$p_{s,i} = \alpha_{s,i} \rho_{s,i} \Theta_{s,i} + \sum_{j=1}^{N-1} 2 \frac{d_{s,j,s,i}^3}{d_{s,i}^3} (1 + e_{s,j,s,i}) g_{0,s,j,s,i} \alpha_{s,i} \alpha_{s,j} \rho_{s,i} \Theta_{s,i}, \quad d_{s,j,s,i} = \frac{d_{s,j} + d_{s,i}}{2} \quad (12)$$

$$\text{Radial distribution function (Ogawa et al., 1980)} \quad g_{0,s,i,s,j} = \frac{d_{s,j} g_{0,s,i,s,j} + d_{s,i} g_{0,s,j,s,i}}{d_{s,j} + d_{s,i}}, \quad g_{0,s,i,s,i} = \left[1 - \left(\frac{\alpha_s}{\alpha_{s,\max}} \right)^{\frac{1}{3}} \right]^{-1} + \frac{1}{2} d_{s,i} \sum_{j=1}^N \frac{\alpha_{s,j}}{d_{s,j}}, \quad \alpha_s = \sum_{j=1}^N \alpha_{s,j} \quad (13)$$

Interphase exchange coefficient for gas–solid interaction (Gidaspow, 1994)

$$K_{s,ig} = \begin{cases} \frac{3}{4} C_D \frac{\alpha_{s,i} \alpha_g \rho_g |\vec{v}_{s,i} - \vec{v}_g|}{d_{s,i}} \alpha_g^{-2/65}, & \alpha_g > 0.8 \\ 150 \frac{\alpha_{s,i} (1 - \alpha_g) \mu_g}{\alpha_g \mu_{s,i}^2} + 1.75 \frac{\rho_g \alpha_{s,i} |\vec{v}_{s,i} - \vec{v}_g|}{d_{s,i}}, & \alpha_g \leq 0.8 \end{cases} \quad (14)$$

$$\text{Drag coefficient } C_D = \frac{24}{\alpha_g R_{e_{s,i}}} \left[1 + 0.15 (\alpha_g R_{e_{s,i}})^{0.687} \right] \quad (15)$$

$$\text{Reynolds number } R_{e_{s,i}} = \frac{\alpha_g \rho_g d_{s,i} |\vec{v}_{s,i} - \vec{v}_g|}{\mu_g} \quad (16)$$

Interphase exchange coefficient for two solid granular phases (Syalmal, 1987)

$$K_{s,i,s,j} = \frac{3 (1 + e_{s,i,s,j}) (0.5\pi + 0.125\pi^2 C_{fr,s,i,s,j}) \alpha_{s,i} \rho_{s,i} \alpha_{s,j} \rho_{s,j} (d_{s,i} + d_{s,j})^2 g_{0,s,i,s,j}}{2\pi (\rho_{s,i} d_{s,i}^3 + \rho_{s,j} d_{s,j}^3)} |\vec{v}_{s,i} - \vec{v}_{s,j}| \quad (17)$$

Diffusive of granular energy coefficient (Gidaspow, 1994)

$$k_{\Theta_{s,i}} = \frac{150 \rho_{s,i} d_{s,i} \sqrt{\Theta_{s,i} \pi}}{384 (1 + e_{s,i,s,i}) g_{0,s,i,s,i}} \left[1 + \frac{6}{5} \alpha_{s,i} g_{0,s,i,s,i} (1 + e_{s,i,s,i}) \right]^2 + 2 \rho_{s,i} \alpha_{s,i}^2 d_{s,i} (1 + e_{s,i,s,i}) g_{0,s,i,s,i} \sqrt{\frac{\Theta_{s,i}}{\pi}} \quad (18)$$

$$\text{Energy dissipation (Lun et al., 1984)} \quad \gamma_{\Theta_{s,i}} = \frac{12 (1 - e_{s,i,s,i}) g_{0,s,i,s,i}}{d_{s,i} \sqrt{\pi}} \rho_{s,i} \alpha_{s,i}^2 \Theta_{s,i}^{\frac{3}{2}} \quad (19)$$

Transfer of the kinetic energy of random fluctuations in particle velocity (Gidaspow, 1994)

$$\phi_{g,s,i} = -3 K_{g,s,i} \Theta_{s,i}, \quad \phi_{s,j,s,i} = -3 K_{s,j,s,i} \Theta_{s,i} \quad (20)$$

$$\text{Heat transfer coefficient between solid and gas phases } h_{s,ig} = \frac{\kappa_g \text{Nu}_{s,i}}{d_{s,i}} \quad (21)$$

Nusselt number (Gunn, 1978)

$$\text{Nu}_{s,i} = (7 - 10\alpha_g + 5\alpha_g^2) \left(1 + 0.7 \text{Re}_{s,i}^{\frac{1}{5}} \text{Pr}^{\frac{1}{3}} \right) + (1.33 - 2.4\alpha_g + 1.2\alpha_g^2) \text{Re}_{s,i}^{\frac{7}{10}} \text{Pr}^{\frac{1}{3}} \quad (22)$$

$$\text{Prandtl number } \text{Pr} = \frac{C_p g \mu_g}{\kappa_g} \quad (23)$$

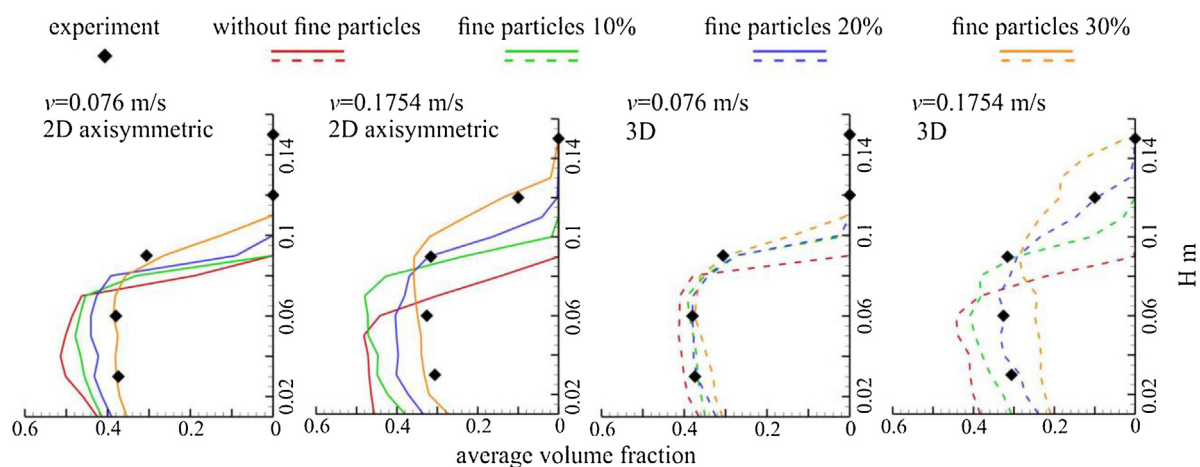


Fig. 2 – Particle volume fraction for particles size test. (For interpretation of the references to colour in the text, the reader is referred to the web version of this article.)

et al., 2012; Nosrati et al., 2018). The same catalyst with the weight of 30 g is put inside the tube. Experiments were conducted for two velocities: 0.076 m/s and 0.1754 m/s.

We have performed two classes of simulations: 2D axisymmetric simulation and full 3D simulation (Fig. 2). A large-scale

reactor is calculated in a 2D axisymmetric approximation. 3D modeling is carried out for comparison since it is feasible for a laboratory experiment in a small tube.

Because of the small sizes of the tube, the size of the mesh has been set to 1 mm and time step to 0.0001 s. The results of

Table 3 – Monitoring the absolute errors of solid particle volume fraction in CFD simulation test.

Velocity, m/s	Height, m	Fine particles volume fraction, %	2D axisymmetric simulation error	3D simulation error
0.076	0.03	0	0.1275	0.0264
0.076	0.06	0	0.1055	0.0313
0.076	0.09	0	0.3060	0.3060
0.076	0.03	10	0.0819	0.0058
0.076	0.06	10	0.0871	0.0072
0.076	0.09	10	0.3060	0.0298
0.076	0.03	20	0.0582	0.0037
0.076	0.06	20	0.0605	0.0010
0.076	0.09	20	0.2163	0.0311
0.076	0.03	30	0.0051	0.0448
0.076	0.06	30	0.0060	0.0050
0.076	0.09	30	0.0414	0.0080
0.1754	0.03	0	0.1627	0.1024
0.1754	0.06	0	0.1159	0.1170
0.1754	0.09	0	0.3160	0.3132
0.1754	0.12	0	0.1012	0.1012
0.1754	0.03	10	0.1431	0.0518
0.1754	0.06	10	0.1459	0.0824
0.1754	0.09	10	0.0771	0.0202
0.1754	0.12	10	0.1008	0.1009
0.1754	0.03	20	0.0955	0.0221
0.1754	0.06	20	0.0781	0.0059
0.1754	0.09	20	0.0062	0.0242
0.1754	0.12	20	0.0982	0.0058
0.1754	0.03	30	0.0261	0.07139
0.1754	0.06	30	0.0230	0.0772
0.1754	0.09	30	0.0412	0.0296
0.1754	0.12	30	0.0364	0.0857

the calculations for the monodisperse catalyst with particles of 100 μm are in red. The data for monodisperse catalyst do not match properly the experimental data. Overall, we see that all the 3D simulations are closer to the experimental results than the 2D axisymmetric simulations.

Then additional calculations were conducted for a bidisperse catalyst for fine particles with the size of 50 μm and volume fraction 10%, 20% and 30% (green, blue and orange lines accordingly). The size of 50 μm was chosen because in the reactor there are filters capturing all particles with the size more than 45 μm and returning them back into the system. Particles with the size less than 45 μm are taken off the reactor's system. Therefore, the smallest particles have the size of 50 μm.

The discrepancy between curves increases with the velocity; at lower velocity curves are closer. Also, the results of monitoring the absolute errors of particle volume fraction between the CFD simulation data and the experimental data are presented in Table 3.

Full 3D simulations exhibit better result than 2D axisymmetric simulations. It appears that in both cases the best approximation is achieved using fine particles 20% in full 3D simulation. Considering only 2D axisymmetric calculations, the best approximation appears to be with volume fraction 30%. On the base of these considerations, the calculations of the large reactor were conducted with the presence of fine particles.

CFD test simulation shows that the presence of fine particles contributes to the fluidized bed expansion and the decrease in the average solid phase volume fraction in the bed.

The porosity of the solid phase decreases, which agrees with the results of (Yates and Newton, 1986; Kono et al., 1987; van Ommen et al., 2007; Gu et al., 2016).

2.5. Mesh size

The entire large-scale reactor computational domain, shown in Fig. 1, is divided into elements of a rectangular shape, the sizes of which are sufficient to determine characteristic factors of the investigated phenomenon. In the calculations carried out in this paper the typical number of finite elements was 465,000. Here we have a hybrid grid with the cell size of 5 mm in the area of the grids near the walls and nozzles and cell size of 10 mm in the reactor free zone. Reducing the cell size will be too expensive in terms of computational cost.

To select a time step, we estimate the Courant number

$$N_C = \frac{|\vec{v}| dt}{dx}. \quad (24)$$

At a given gas flow rate, the average velocity in reactor section is 0.32 m/s. Fig. 3 shows the calculations for the average values of particle volume fraction along the height of the reactor near the central pipe, between the pipe and the wall, and near the wall. In the calculations, the time steps are 0.01 s, 0.005 s, 0.001 s, 0.0005 s and 0.00025 s. The averaging is taken from five calculations for each step in interval time of 60–70 s of the reactor operation.

We can see a change in the height of the bed and its average volume fraction with a change in the time step in Fig. 3a. Step 0.01 s causes oscillations in the height of the bed. Step 0.001 s gives a more uniform particle volume fraction along the height of the bed on all calculated lines.

A time step of 0.01 s provides a criterion for the Courant number of 0.32 and 0.64 for a mesh size of 10 mm and 5 mm respectively. The authors (Gobin et al., 2001) proposed a maximum Courant number of 0.3. For monodisperse liquid–fluidized suspensions, authors (Cornelissen et al., 2007) suggested setting a limit on a Courant number between 0.03 and 0.3. For such values, the time step should be in the range from 0.00046 to 0.009.

Fig. 3b presents comparative calculations for the time step of 0.001 s, 0.0005 s and 0.00025 s. It can be seen that there are small differences, but the behavior is the same, there are no oscillations. At the same time, the choice of time less than 0.001 s will be too expensive in terms of computational time. Thus, a hybrid mesh with cells of size 5 mm and 10 mm and the time step of 0.001 s was chosen for the calculations.

2.6. Boundary and initial conditions

The boundary conditions were set according to the mechanics of the reactor's work and the solver used at all the boundaries of the calculation domain. As the reactor model assumes rotational symmetry, the condition of axial symmetry “axis” was set on the axis of the constructed model. The “wall” conditions were set at all impermeable surfaces; temperature equal to the temperature of the supplying catalysts was set on the wall of the pipe to supply fresh catalyst, while other walls were considered thermally insulated. “Velocity-inlet” conditions were set for the models of gas–raw supply nozzles and for the outlet of the centrally located pipe of the catalyst supply. Velocities were specified according to the gas and the catalyst flow rate required. The temperatures of gas and catalyst were

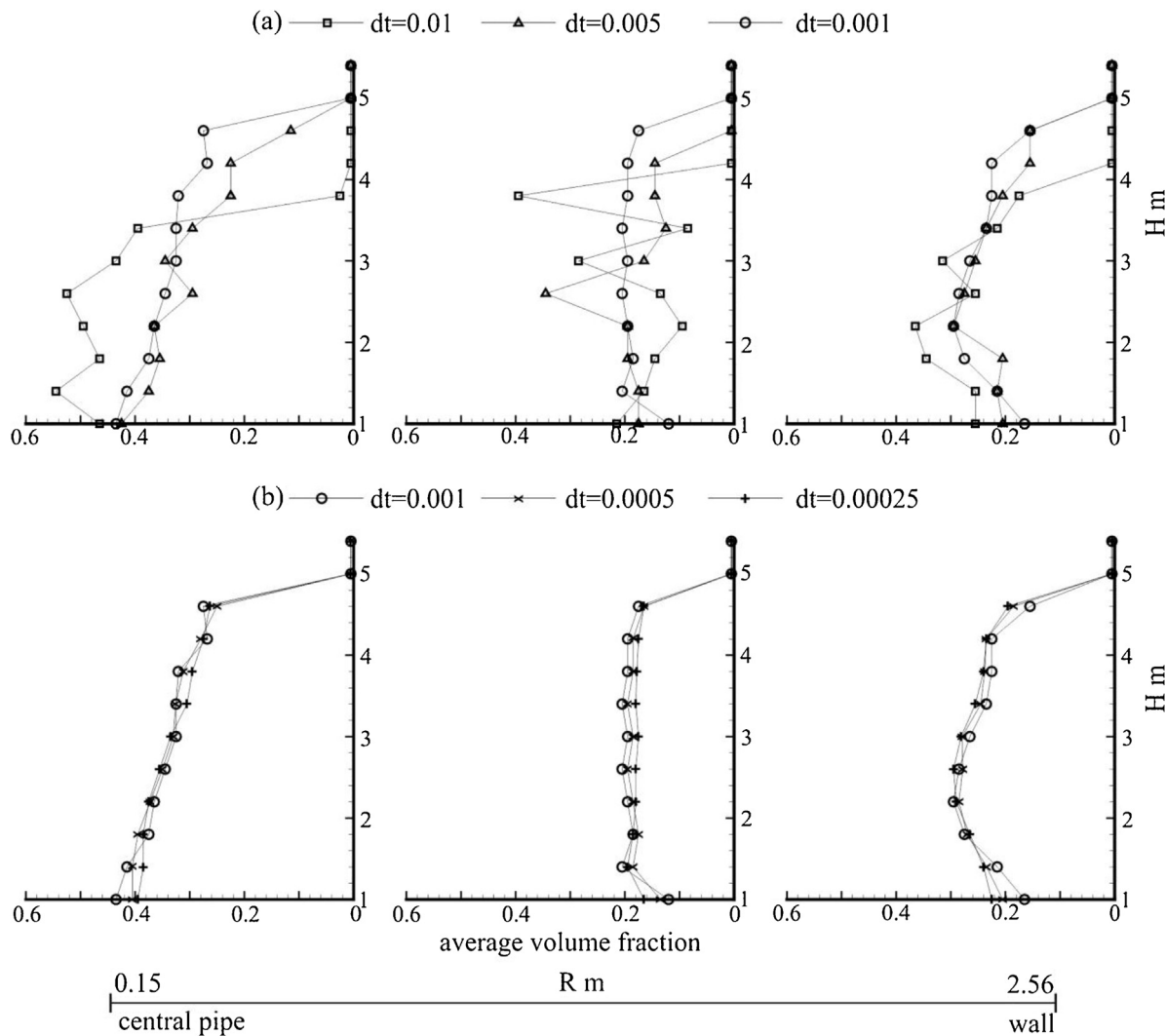


Fig. 3 – Particle volume fraction on test vertical lines.

Table 4 – Operating conditions for the reactor model.

	Gas	Catalyst
Density (kg/m^3)	1	2400
Viscosity ($\text{kg}/(\text{m s})$)	$1e-05$	–
Thermal conductivity ($\text{W}/(\text{m K})$)	0.013258	37
C_p (specific heat) ($\text{J}/(\text{kg K})$)	2680	1047
Mass flow rate (kg/s)	6.6	20.6
Coarse particle diameter (μm)	–	100
Fine particle diameter (μm)	–	50

set to 550 °C and 650 °C, respectively. “Pressure-outlet” conditions were specified on a site at the upper part of the reactor model for a gas outlet, and on the site at the bottom part of the reactor to simulate the flow of catalyst into the regenerator. Also, there is a removal of the catalyst fine particles through the outlet at the reactor top part. In the current reactor, particles from the upper part turn back into the working area under the grids through cyclones. In the model constructed “velocity-inlet” conditions were specified on the output channels of cyclones according to a flow rate of catalyst through the outlet channel in the upper part of the reactor.

The final properties of the gas and the catalyst used are shown in Table 4. The rates are selected from the industrial parameters 24 t/h and 72 t/h, respectively, for gas and catalyst. Due to the small number of impurities in the feed gas raw materials, they can be considered as homogeneous. From

the fractional composition analysis of the catalyst used in the reactors, the two fractional models are assumed for calculations.

At the gas flow rate under consideration the terminal velocity for coarse particles is $U_t(d_p = 100 \mu\text{m}) = 0.99 \text{ m/s}$ and for the fine particles is $U_t(d_p = 50 \mu\text{m}) = 0.29 \text{ m/s}$. Thus, coarse particles must form a bounded bed, while the fine particles move throughout the entire volume of the reactor and are carried out of it.

After the setting of the initial distribution of catalyst in the reactor solving the equations was started on the built mesh. After some period, the flow in the constructed model reached the quasi-stationary mode, which was assumed as the hydrodynamic and thermal picture of the reactor’s operation in the approximation of the constructed model. Time to reach the quasi-steady mode of the calculation depended on the conditions of the computational experiment and on average took about 50 s of actual time.

3. Results

3.1. Analysis of the reactor operation

Fig. 4 shows the characteristic patterns of the catalyst particle volume fraction and gas temperature in the reactor for monodisperse and bidisperse cases. This figure corresponds

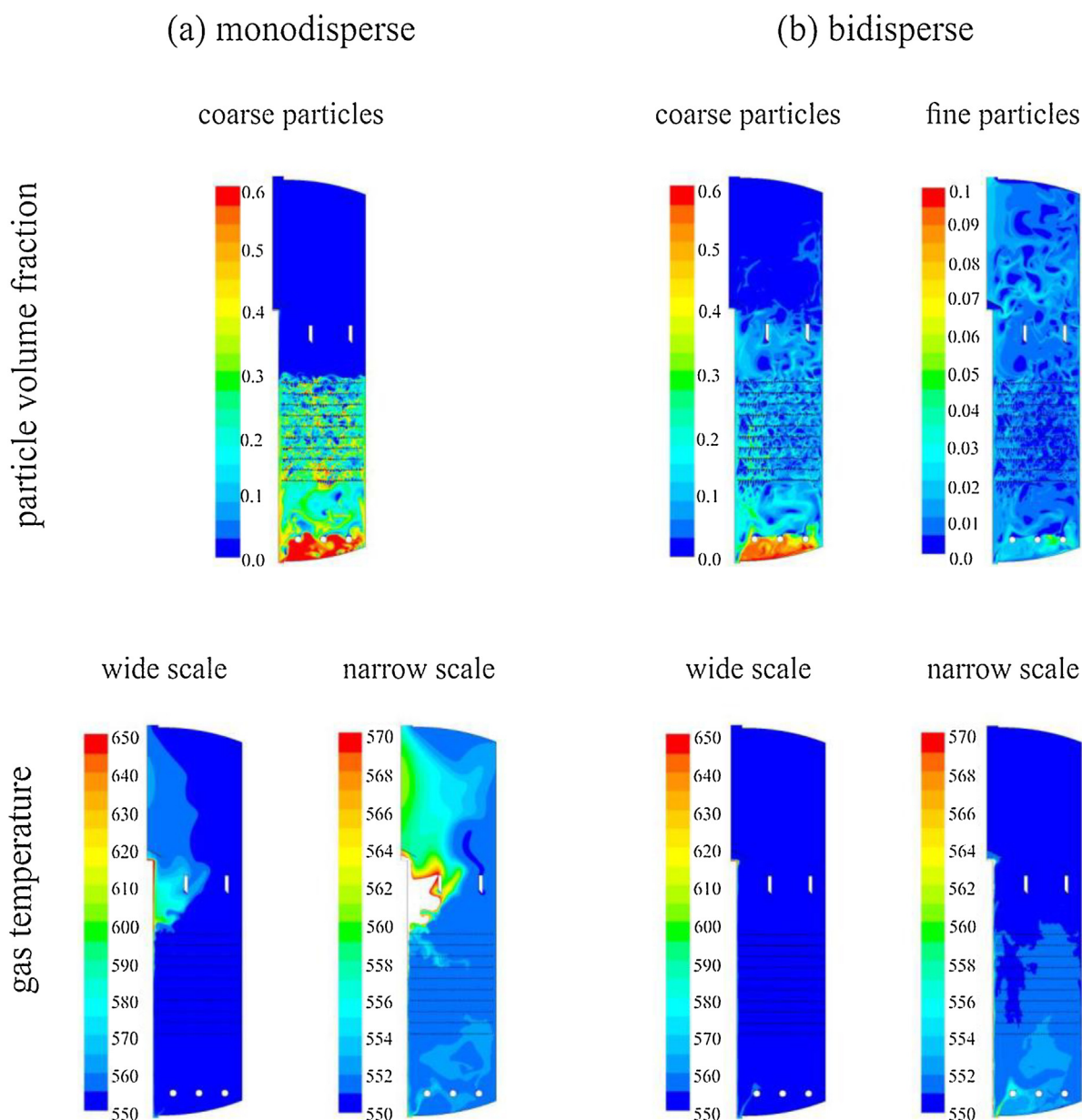


Fig. 4 – The catalyst volume fraction and gas temperature fields in the reactor. Coarse particle (100%) volume fraction is presented for the monodisperse case (a). Coarse (65%) and fine (35%) particle volume fraction is presented for bidisperse case (b). Temperature fields are presented in the wide-scale 550–650 °C and the narrow scale 550–570 °C.

to the instantaneous state after a one minute of the real-time operation and is characterized by the presence of the areas of low concentrations (gas bubbles) and the areas of high concentrations (catalyst clots).

In the case of monodisperse fluidized bed, the particle size is chosen to consider the fact that the average gas velocity is not sufficient for the catalyst grains removal. This ensures the presence of an expanded bed height in numerical simulation. For calculating the bidisperse catalyst coarse and fine particle sizes are chosen in a proportion of 65% and 35% of volume fraction, respectively. The fine particles are presented in the whole reactor area with small volume fraction. Also, the presence of fine particles contributes to the fluidized bed expansion.

The studied chemical reaction rate depends on the temperature and starts with heat absorption. In order to maintain the temperature, sufficient for the reaction, the heated catalyst is continuously fed to the reactor from the regenerator. In calculations of the reactor model, the gas feed temperature was set to 550 °C, and regenerated catalyst was fed at

a temperature of 650 °C. The change in of the temperature due to the chemical reaction is not taken into account. The heat exchange between the catalyst entered, the gas and the circulating catalyst is only considered. Despite the fact that the calculation does not take into account the temperature effects of the reactions, the nature of heat propagation from the incoming field the catalyst will most likely determine the reaction.

The gas temperature fields are shown in Fig. 4 in two scales: wide scale from 550 to 650 °C and a narrow scale from 550 to 570 °C. When considering the wide scale in the monodisperse case, a region of notable gas heating near the regenerated heated catalyst feeder is observed. In that region, there is no catalyst, and the rising gas takes heat from the incoming catalyst granules. In the bidisperse case, notable heating zones are not observed on the wide range.

A narrow scale makes it possible to determine the zones of the initial reactor heating. A white spot appeared in the picture for the case of monodisperse particles. This is an area

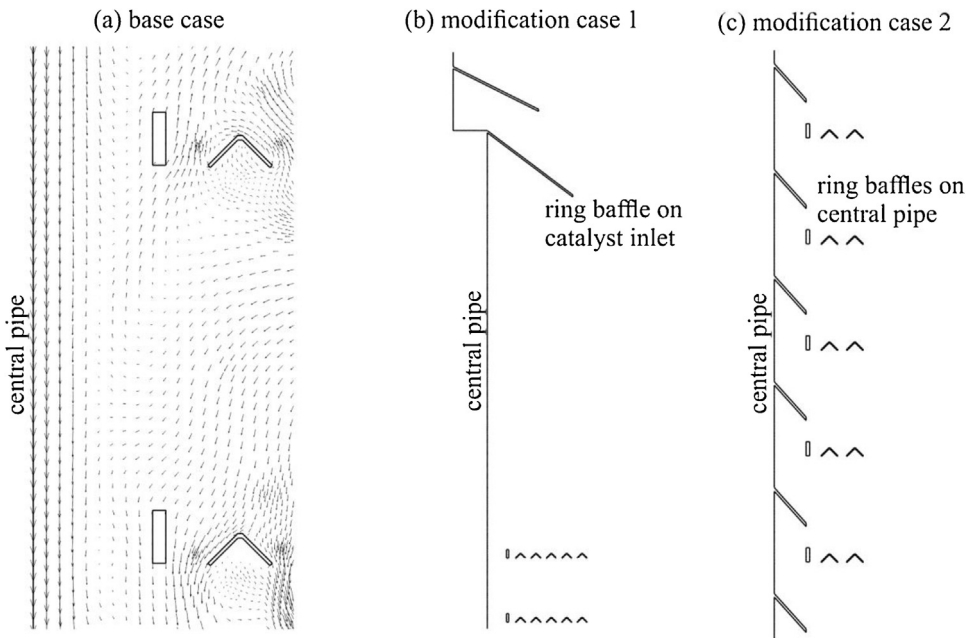


Fig. 5 – Particle motion along the central vertical pipe (a) and modification case 1 (b) and case 2 (c).

where the temperature is higher than 570 °C. In general, it can be seen that the gas is more heated in the upper part of the reactor, where there is no catalyst. But the lower part of the reactor is also warming up. For the bidisperse case, the gas is more heated in the lower part of the reactor where the catalyst particles are located.

3.2. Particles motion near the hot catalyst feeder and the central pipe

In the currently operating reactors, the gap between the wall of the reactor and the grids has a significant effect on the catalyst circulation. In the calculations carried out along the wall of the reactor and along the central pipe of catalyst feeder we observed significant descending flows of catalyst particles (Fig. 5a). The presence of the circulation mechanism in the reactor has a positive effect on the course of chemical reactions, as there is an active catalyst mixing over the entire reactor height. The reactor is connected with the regenerator by two cross flows, where the spent catalyst should fall and the fresh catalyst is supplied into the reactor. The incoming fresh catalyst has a higher temperature and hence can more actively participate in chemical reactions. Therefore, the type of the distribution of fresh hot catalyst incoming to the reactor is of a great importance.

In the numerical simulation of the monodisperse catalyst case, considerable heating begins in the upper part of the reactor. The upward flow of the gas, which is moving towards the outlet from the reactor, is warming up considerably. When calculating the case of the bidisperse catalyst (used in industrial reactors), the heating starts at the bottom of the reactor. This may be due to the downward flow of hot particles along the central pipe from the catalyst feeder outlet to the bottom of the reactor. This may not be effective since the channels are situated in the lower part for removing the catalyst from the reactor. Therefore, in the industrial reactors, it is desired to warm up the middle part of the reactor, where grids are installed.

Considering the gas temperature fields, catalyst volume fraction fields, and the patterns of particle motion vectors,

the following assumptions can be made. The incoming hot catalyst falls on the fluidized bed in monodisperse case. Hot particles give off heat to the upward gas flow. The incoming hot catalyst moves along the central pipe from top to bottom in bidisperse case. Once under the gas feeder on the bed of a dense catalyst, the heated particles give off heat more poorly than in the monodisperse case, as it is seen in Fig. 4. The redirection of this particular particle flux can influence the location of the initial heating zones.

Let us consider the options for modifying the reactor block, based on the analysis of the calculation results obtained.

3.3. Modification case 1

As the first modification option, we will consider the change in the heated catalyst feed device. In the model of the device, we will set a baffle whose geometric interpretation is shown in Fig. 5b. This option may not be unique, and it implies a device that increases the area for the distribution of the catalyst feed. A deflector mounted at the exit of the pipe allows to reduce the downward flow and direct the heated catalyst into the upper reactor zone.

Fig. 6 shows catalyst volume fraction fields calculated with adding this modification into the construction of the catalyst feeder. There are no differences in the distribution of the catalyst in the bed. This is due to the fact that the amount of catalyst fed is small compared to the catalyst in the circulating bed. Incoming catalyst has little effect on the hydrodynamics of the reactor bed core.

Fig. 6 also shows calculated gas temperature fields. However, in a modified case there is a large area of a white color corresponding to a range from 570 °C to 650 °C for the monodisperse catalyst. If we add the deflector the heat of the reactor's upper region is greatly increased. Hot catalyst does not roll down along the pipe and reaches the upper boundary of the bed while maximally exchanging heat with ascending gas flows.

For a bidisperse catalyst, a significant part of the fresh heated catalyst also falls into the zone of fine particle's circulation, where it starts the processes of heat transfer to the

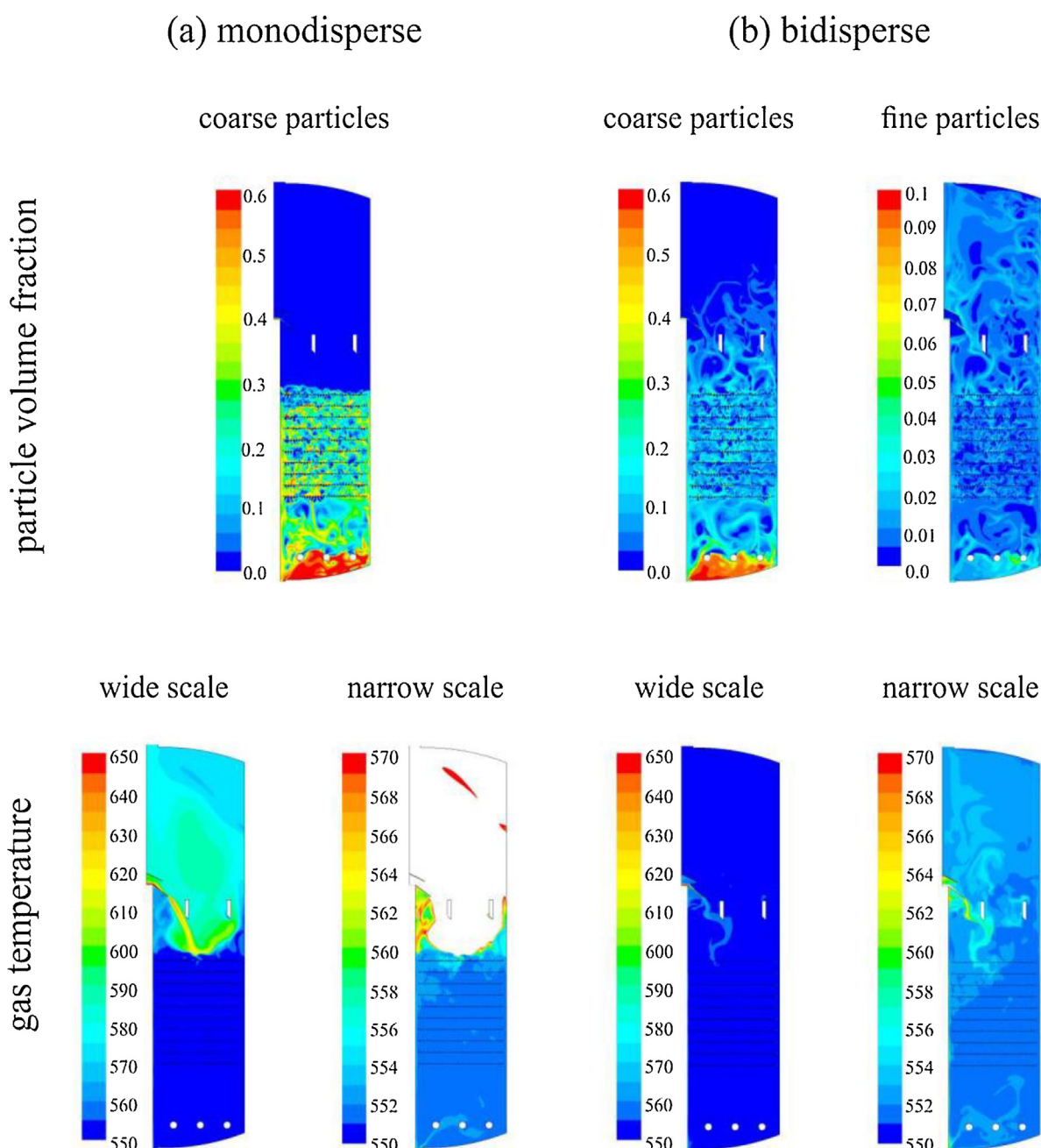


Fig. 6 – The catalyst volume fraction and gas temperature fields in the reactor for modification 1. The coarse particle volume fraction is presented for the monodisperse case (a). Coarse and fine particle volume fraction is presented for the bidisperse case (b). Temperature fields are presented in the wide-scale 550–650 °C and the narrow scale 550–570 °C.

circulating bed and gas. In comparison to the base case, there is a considerable heating of the areas of the upper and higher grids. In terms of heating reactant gas-feed, the use of such modification has a positive effect. When the fine and coarse particles are in the heated region they participate in a chemical reaction.

3.4. Modification case 2

The desired modification goal is to direct the heated catalyst particles into the reactor region where a large amount of catalyst is located. In the reactor under consideration, this is a region with grids. There are coarse catalyst particles. We can use deflectors to direct the hot particles flow into the grid area. For example, in articles (Golriz and Grace, 2002;

Samruamphianskun et al., 2012; Chalermisinsuwan et al., 2014; Guio-Perez et al., 2013; Guio-Perez et al., 2014; Rossbach et al., 2016) ring baffles are used on the walls. It is noted that the ring baffles improve the phases mixing in the radial direction and the elimination of the reverse flow near the wall, which allows obtaining a high benefit for heat and mass transfer. Also, the particle residence time in zones with installed internals is increased. The numerical results obtained show that ring baffles improve the homogeneity of the gas–solid flow, which makes the use of ring baffles suitable. In our unit, such internals can also increase the heat exchange between the heated central pipe and the phases in the reactor.

As the second modified scheme, we propose to eliminate the downward flows of the heated catalyst along the pipe and to direct the catalyst into the space between the grids.

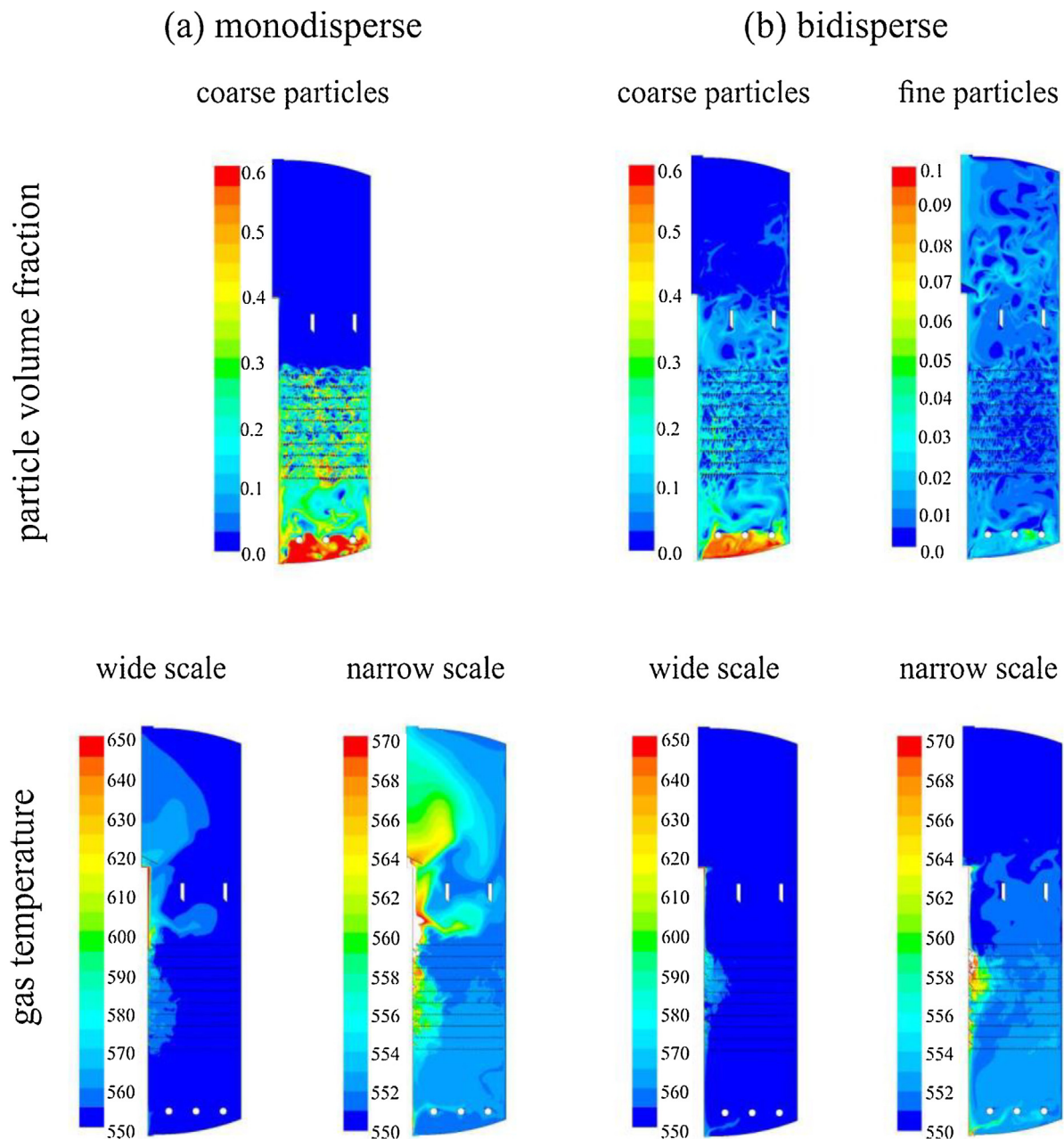


Fig. 7 – The catalyst volume fraction and gas temperature fields in the reactor for modification 2. The coarse particle volume fraction is presented for the monodisperse case (a). Coarse and fine particle volume fraction is presented for the bidisperse case (b). Temperature fields are presented in the wide-scale 550–650 °C and the narrow scale 550–570 °C.

This scheme allows heating the zones with a higher catalyst volume fraction. To implement this idea we conducted the calculations with the baffles disposed on the pipe. The realization of the idea is shown in Fig. 5c. Note that the elimination of downward flows along the pipe will not lead to a violation of the particle circulation mechanism. The volume of catalyst, falling down along the pipe, is averagely a tenth part of the catalyst volume, descending along the walls of the reactor. Therefore, the overall circulation of the catalyst in the reactor is not disturbed.

Calculations of monodisperse and bidisperse fluidized bed were carried out for the model constructed. Fig. 7 shows the catalyst volume fraction and gas temperature fields. The catalyst volume fraction fields also do not differ much from the base case and modification 1. However, the gas temperature fields have significant differences from the cases considered previously. An increase in temperature in the grid zone near

the central pipe is seen in both cases of the monodisperse catalyst numerical simulation and the bidisperse catalyst numerical simulation. It can have a beneficial effect since there is a large number of coarse catalyst particles in that zone.

4. Summary

4.1. Particle circulation in the reactor

From the results described, we can see that the existence of fine particles has an impact on the circulation in the fluidized bed of the reactor as well as on the temperature field. This is primarily due to the movement of the particles in the top of the reactor. However, a bed of coarse catalyst particles circulating in the middle part of the reactor makes a significant contribution to the efficiency of the reactor.

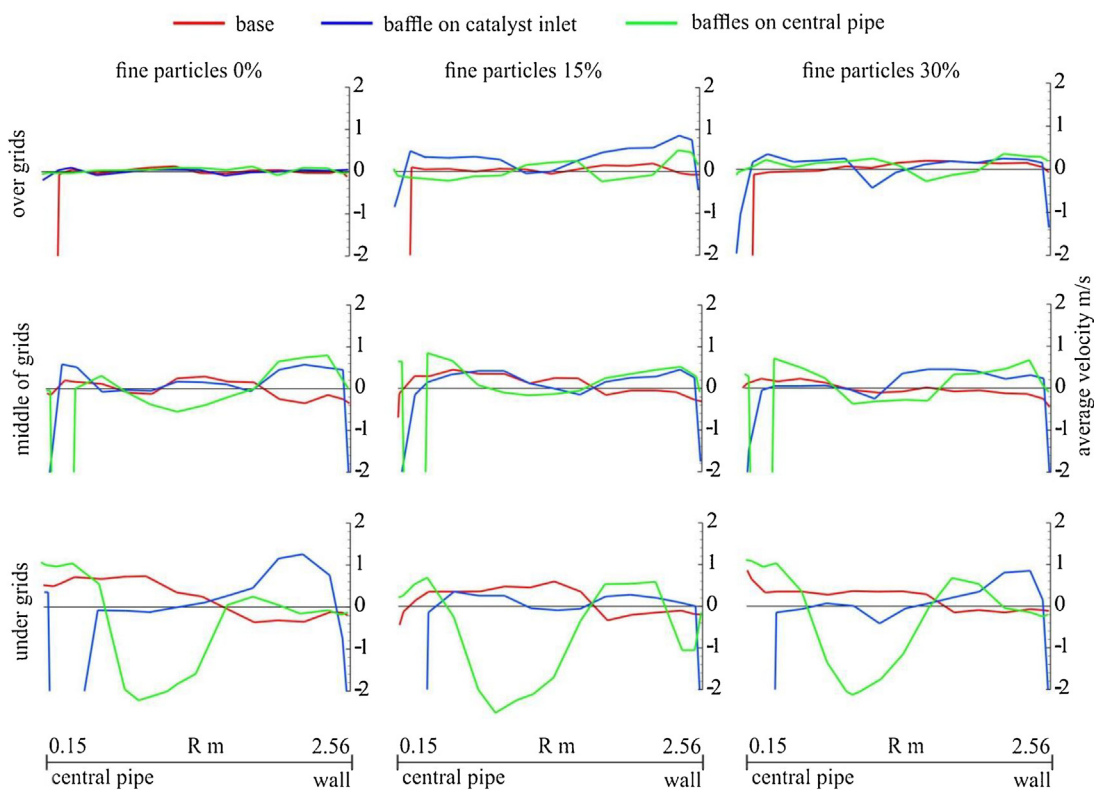


Fig. 8 – Average velocities of the particle movement in the middle part of the reactor. (For interpretation of the references to colour in the text, the reader is referred to the web version of this article.)

To better understand the impact of the modifications proposed we constructed the average values of the catalyst particles and gas velocities' vertical components. The average values are taken from the five single calculations over the time interval of 60–70 s. The results are shown in Fig. 8. The curves are obtained for the points over the top grid, between the middle grids, and under the bottom grid with a fine particle of 0%, 15% and 30%.

It is seen from the figure that on the upper grid in all the cases circulation flows are not yet clearly expressed. Only in the case of modification 1 with the baffle on the central pipe, there is a flexure in the middle of the curve that indicates the hitting place of the particles received from the regenerator to the main catalyst bed. Red lines represent the curves for the base case of the reactor. The downward flow of particles along the wall becomes especially important to the bottom grids, creating a global circulation flow from the rolling of the particles in a large area near the wall and lifting the particles closer to the axis of the reactor. At the same time, there is a thin bed of particles descending along the central pipe.

Blue lines represent the curves for modification 1 with the baffle on the catalyst inlet. The curve of the mean velocities describes two significant downward flows along the wall and along the central pipe. The flexure at the center is defined by the movement of particles received from the regenerator. In other zones, particles are raising up.

Green lines represent the curves for modification 2 with the baffles along the central pipe. Several opposing flows of high intensity are observed. Particles move down along the wall of the reactor, then there follows the zone of particles moving up, and a significant zone of descending particles, after which again we have a zone of the particles rising up. Continuous flow along the center pipe

is not possible due to the presence of deflectors. Small circulation zones are observed between the baffles along the pipe.

4.2. Average catalyst volume fraction and gas temperature

The average parameters of catalyst volume fraction and gas temperature are presented below. The average values are taken from five single calculations for the time moment of 60 s of reactor operation. In Fig. 9 we can see the curves for the parameters under the grids, in the middle zone of the grids and above the grids, depending on the percentage of fines. The catalyst volume fraction is approximately the same for the base case and modifications. It can be seen that the total particle concentration decreases between the grids as the fine particles percentage increase. Fine particles are easier to slip through the free cross-section of the grids, and also they circulate throughout the entire height of the reactor. In modification 2, we eliminated the flows along the pipe, sending the particles into the grid zone. Thus, we raised the gas temperature between the grids and under the grids.

Fig. 10 shows the average parameters along the vertical lines: along a pipe near the symmetry axis, in the middle between the pipe and the wall, near the wall. The particle volume fraction along vertical lines is approximately the same in all cases. There is a decrease in concentration near the pipe for modification 2 with baffles. There is no dense downward flow. The gas temperature is expected to increase along the pipe for modification 2 and decreases with modification 1. In this case, modification 1 shows a significant increase in gas temperature closer to the wall with an increase of the fine particles fraction percentage.

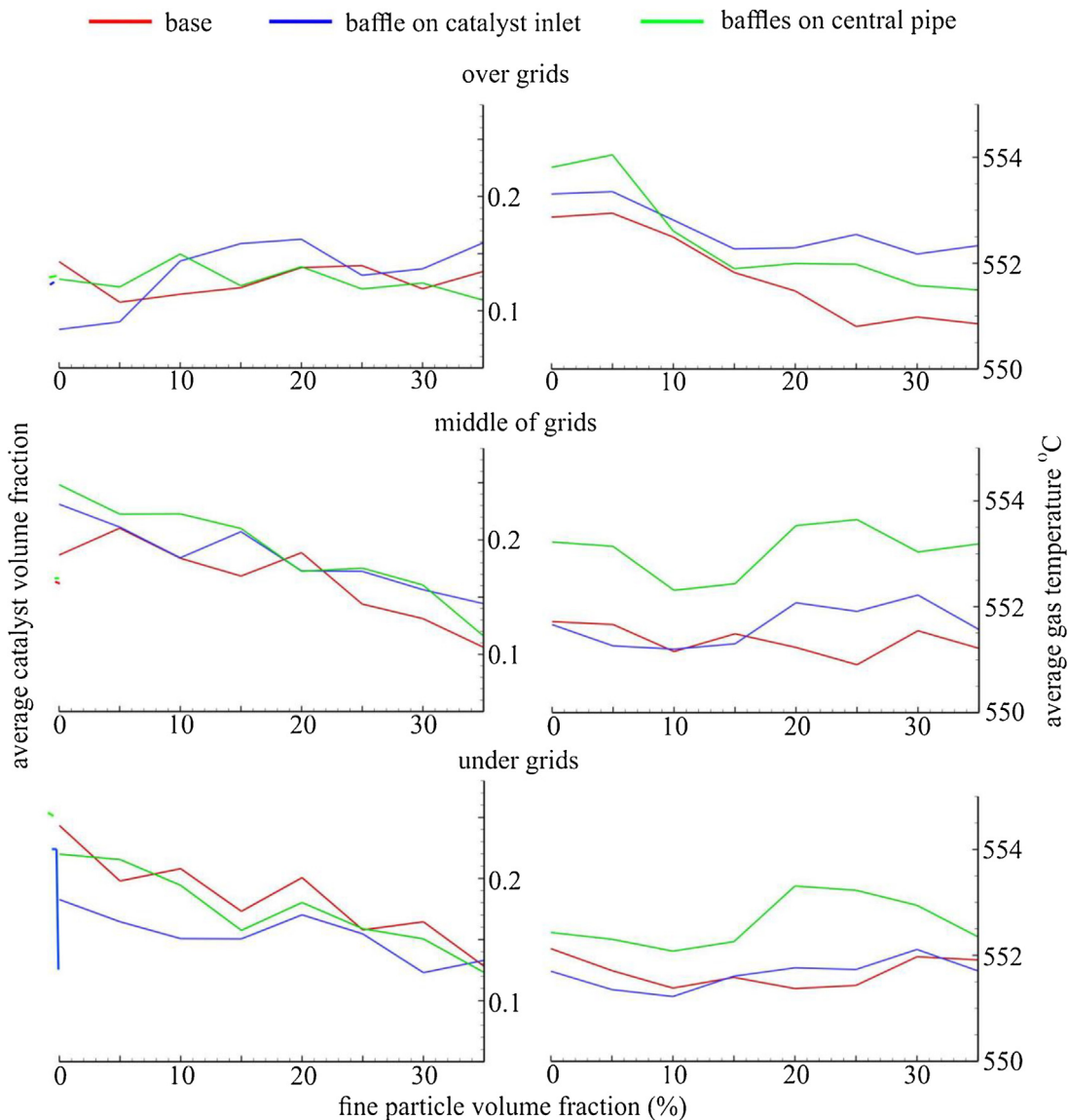


Fig. 9 – Average values of catalyst volume fraction and gas temperature in the middle part of the reactor. (For interpretation of the references to colour in the text, the reader is referred to the web version of this article.)

4.3. Average gas temperature and added enthalpy rate in the reactor

Then we analyze the average gas temperature in the reactor. Fig. 11 shows graphs for the operating time of the reactor of 60 (solid lines) and 70 (dashed lines) seconds. The reactor with modification 1 without the fine fraction has the largest average gas temperature. However, as the percentage of fine particles increases, the average gas temperatures approach each other. The resulting graphs are correlated with Figs. 4, 6 and 7. It may seem that the presence of a baffle at the pipe outlet in the absence of fine particles is the most effective option. But in this case, the upper part of the reactor is warmed up, and there are almost no particles. At the same time, the heat received from the catalyst is simply carried out.

For a more effective evaluation of the reactor heating, we calculate the enthalpy flow rate introduced into the reactor as

It can be seen from Fig. 11 that the thermal energy that remains in the reactor is inversely proportional to the average gas temperature in the reactor. The highly heated gas carries a lot of thermal energy out of the reactor. Adding fine particles allows storing more thermal energy in it. Judging by these characteristics, the greatest effect of adding the fine particles is observed for the modification 1 case.

The increase in the flow enthalpy in the reactor with the addition of fine particles can be associated with two factors. First, fine particles are located in the entire volume of the reactor, and coarse particles are mostly below the upper grid. Secondly, the fine particles have a large surface area. In our example, the volume of one granule of a coarse particle is equal to the volume of eight granules of fine particles. The surface area of one granule of a coarse particle is equal to the surface area of four granules of fine particles. Thus, with an equal volume fraction, fine particles will have a surface area twice as large as coarse particles. That is, fine particles can transfer more heat to the gas compared to coarse particles.

$$\dot{h}_{\text{reactor}} = \dot{h}_{\text{gas,inlet}} + \dot{h}_{\text{cat,inlet}} - \dot{h}_{\text{gas,outlet}}. \quad (25)$$

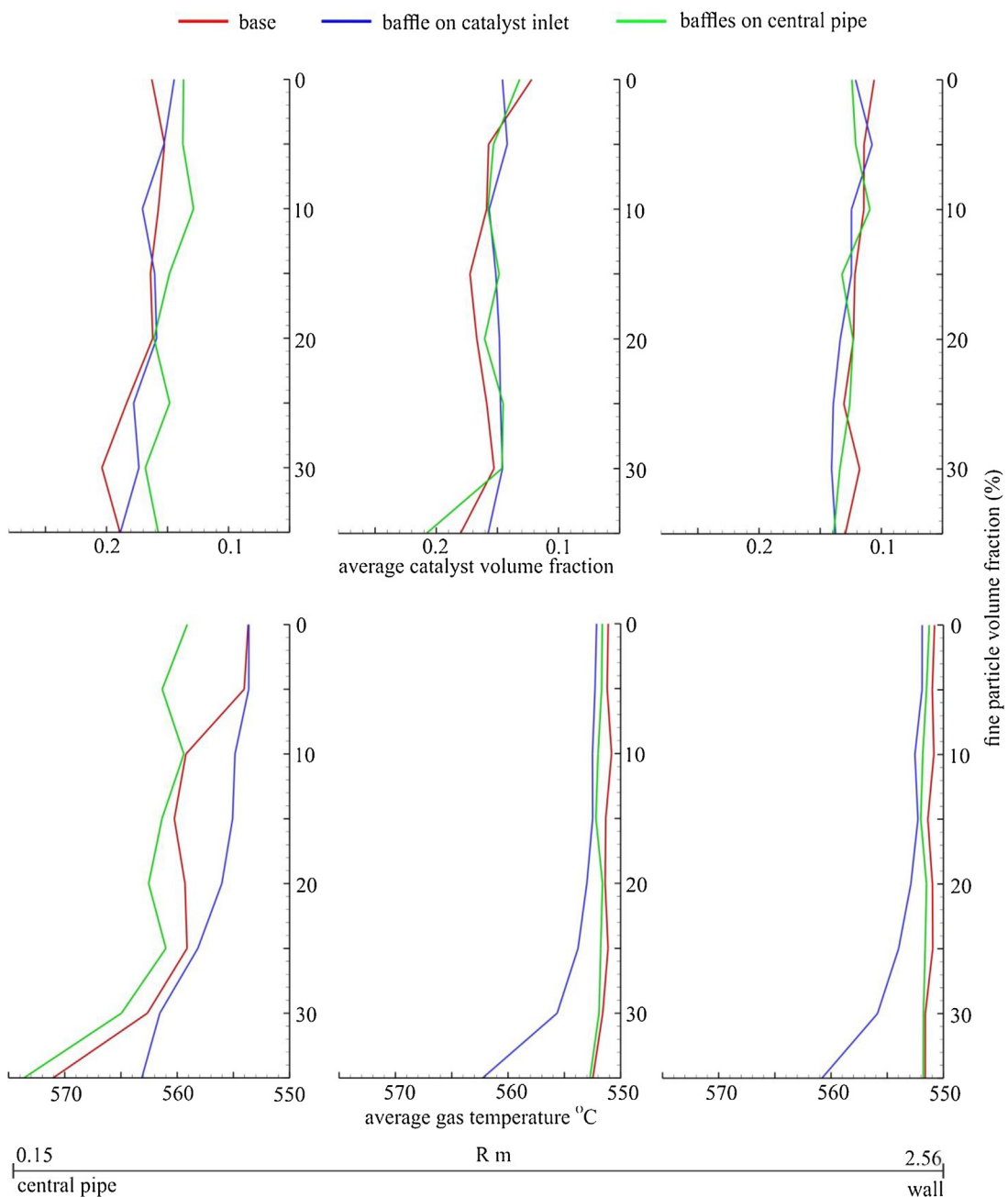


Fig. 10 – Average values of catalyst volume fraction and gas temperature on vertical lines. (For interpretation of the references to colour in the text, the reader is referred to the web version of this article.)

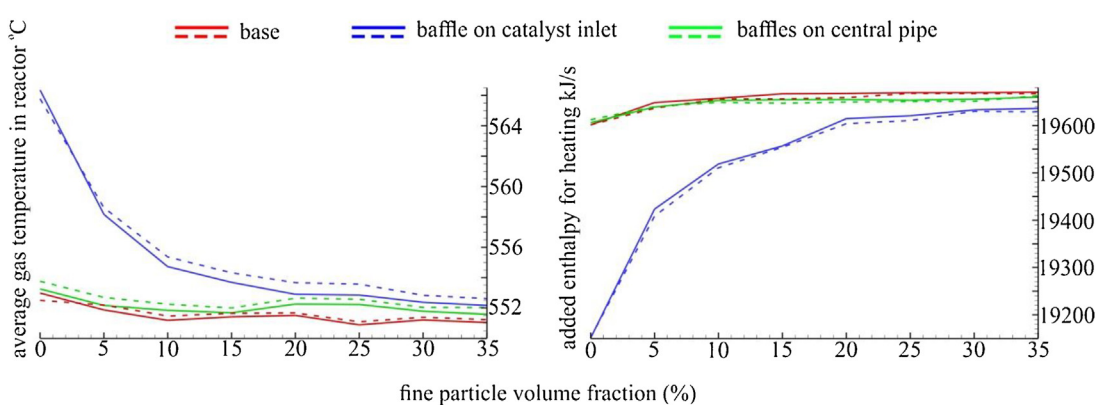


Fig. 11 – Average gas temperature and added enthalpy rate. Solid lines show 60 s of the reactor operation, dashed lines show 70 s of the reactor operation. (For interpretation of the references to colour in the text, the reader is referred to the web version of this article.)

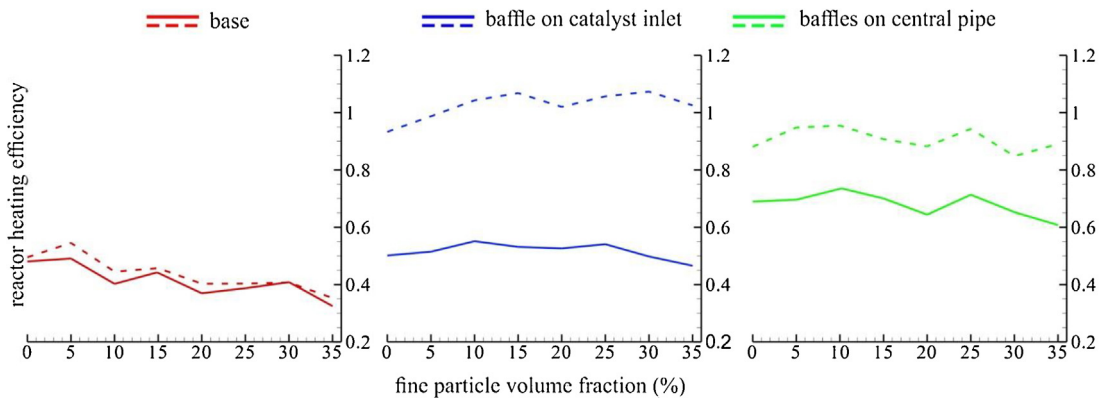


Fig. 12 – The reactor heating efficiency. Solid lines show 60 s of the reactor operation, dashed lines show 70 s of the reactor operation. (For interpretation of the references to colour in the text, the reader is referred to the web version of this article.)

4.4. Reactor heating efficiency

We made one more estimate of the modifications efficiency. By analogy with the paper (Solov'ev et al., 2016) assessment of efficiency was conducted on the basis of the function of reactor heating efficiency

$$F_{ef}(x, y) = \alpha_{cat}(x, y) (T_{gas}(x, y) - T_{gas,0}(x, y)), \quad (26)$$

where $\alpha_{cat}(x, y)$ is the catalyst volume fraction ($\alpha_{cat} = \sum_{i=1}^N \alpha_{s,i}$),

$T_{gas}(x, y)$ is the gas temperature at a point in the reactor. The value $T_{gas,0}(x, y)$ means a minimum temperature at which gas is fed to the reactor. The higher gas temperature and the catalyst concentration in a particular point of the reactor are more likely to cause the reaction at this point. To determine an integral value which characterizes the function of efficiency, we introduce the factor

$$C_{ef} = \frac{\int_V F_{ef} dV}{\alpha_{cat,max} T_{gas,max} V} \cdot 100. \quad (27)$$

The coefficient defined by the Formula (27) characterizes the efficiency of the reactor heating in the entire active reactor zone. The value of $C_{ef}=100$ is only possible if the entire reactor is the most densely filled with the catalyst while the gas is heated to a maximum possible temperature. Of course, in a real reactor, the catalyst is not distributed densely, and the gas is heated irregularly as it passes through the hot catalyst. Therefore, in the real reactor model, the coefficient will be much less than 100.

Fig. 12 shows the graphs for the base case and various modifications suggested by the volume content of fine particles. The solid lines represent the results after 60 s of operation of the reactor, the dashed – after 70 s of the reactor operation.

It is seen that the presence of fine particles, even up to 35% does not greatly change the efficiency of the reactor heating. In the base case block's heating goes very slow, as evidenced by the minor difference of the results for 60 and 70 s of the reactor operation. The efficiency of heating is much higher in the cases with the modifications. This indicates the correct identification of the problems of the base case and of the right idea for optimization by modifying the internal components. The addition of fine particles leads to the more intensive gas heating in the zones with a large number of catalyst particles

and a decrease in the gas temperature in the zones with a small number of catalyst particles.

5. Conclusion

From calculations of the base reactor and proposed variants of the construction changes, we can make conclusions regarding the movement of the catalyst in the reactor, the processes of heat exchange and the reactor heating. In a turbulent gas bed, the catalyst granules form the main circulating flows. A major role here belongs to the parietal effect when the particles fall along the walls at the high speed and rise gradually in the free zones of the apparatus. Grids located in the reactor contribute to the break of rising gas bubbles and mixing of the catalyst grains.

The type and position of the hot particle feeder have a major effect on the rate of the reactor heating and the initial zones of that heating in it. By controlling the direction of hot catalyst granules movement on the output device, it is possible to change the region of the reactor heating based on the necessary conditions. Note that the modifications considered did not change the position of the hot particles feeding point into the reactor, but only redirected the particles.

The presence of fine particles affects the hydrodynamics of the fluidized bed and the reactor heating. The bed expansion is increased, the average value of particle volume fraction in the section is decreased. Numerical simulation results show that the presence of fine particles reduces the average gas temperature in the reactor. However, the presence of fine particles contributes to the conservation of larger amounts of thermal energy in the reactor. Also, the addition of fine particles can change the heating regions in the reactor. In the cases considered, the addition of fine particles contributed to the increase of intensity of the heating of the lower part of the reactor, where coarse particles circulate.

A function is considered that depends on the catalyst particle volume fraction and the gas temperature, to estimate the efficiency of the reactor heating. The function helps to determine when the hot gas is in contact with large volumes of the catalyst. The modifications proposed showed an increase in efficiency, in comparison with the base case. Moreover, the addition of fine particles had a negligible effect on the values of the function under consideration. The addition of fines leads to more intensive gas heating in the zones with a large number of catalyst particles and a decrease in the gas temperature in zones with a small number of catalyst particles.

Thus, the type of the hot catalyst particle feeder and the presence of fine particles can influence the intensity of the reactor heating and the area of strong and weak heating. Note that these results correspond only to the reactor design considered and may not be valid if there are additional structural elements.

Acknowledgements

The reported research was funded by Russian Foundation for Basic Research and the government of the Republic of Tatarstan of the Russian Federation, grant no. 18-48-160006.

References

- Ansart, R., Vanni, F., Caussat, B., Abitzer, C., Brothier, M., 2017. Effects of reducing the reactor diameter on the dense gas–solid fluidization of very heavy particles: 3D numerical simulations. *Chem. Eng. Res. Des.* 117, 575–583.
- Bakshi, A., Altantzis, C., Bates, R.B., Ghoniem, A.F., 2015. Eulerian–Eulerian simulation of dense solid–gas cylindrical fluidized beds: impact of wall boundary condition and drag model on fluidization. *Powder Technol.* 277, 47–62.
- Basu, P., 2006. Combustion and Gasification in Fluidized Beds. CRC press.
- Beetstra, R., Nijenhuis, J., Ellis, N., van Ommen, J.R., 2009. The influence of the particle size distribution on fluidized bed hydrodynamics using highthroughput experimentation. *AIChE J.* 55, 2013–2023.
- Brouwer, G.C., Wagner, E.C., van Ommen, J.R., Mudde, R.F., 2012. Effects of pressure and fines content on bubble diameter in a fluidized bed studied using fast X-ray tomography. *Chem. Eng. J.* 207–208, 711–717.
- Bu, J., Zhu, J., 1999. Influence of ring-type internals on axial pressure distribution in circulating fluidized bed. *Can. J. Chem. Eng.* 77, 26–34.
- Chalermisinsuwan, B., Chanchuey, T., Buakhao, W., Gidaspow, D., Piumsomboon, P., 2012. Computational fluid dynamics of circulating fluidized bed downer: study of modeling parameters and system hydrodynamic characteristics. *Chem. Eng. J.* 189–190, 314–335.
- Chalermisinsuwan, B., Kuchonthara, P., Piumsomboon, P., 2009. Effect of circulating fluidized bed reactor riser geometries on chemical reaction rates by using CFD simulations. *Chem. Eng. Process.* 48, 165–177.
- Chalermisinsuwan, B., Kuchonthara, P., Piumsomboon, P., 2010. CFD modeling of tapered circulating fluidized bed reactor risers: hydrodynamic descriptions and chemical reaction responses. *Chem. Eng. Process.* 49, 1144–1160.
- Chalermisinsuwan, B., Samruamphianskun, T., Piumsomboon, P., 2014. Effect of operating parameters inside circulating fluidized bed reactor riser with ring baffles using CFD simulation and experimental design analysis. *Chem. Eng. Res. Des.* 92, 2479–2492.
- Chen, J., Kemoun, A., Al-Dahhan, M.H., Duduković, M.P., Lee, D.J., Fan, L.-S., 1999. Comparative hydrodynamics study in a bubble column using computer-automated radioactive particle tracking (CARPT)/computed tomography (CT) and particle image velocimetry (PIV). *Chem. Eng. Sci.* 54 (13–14), 2199–2207.
- Chen, X., Wang, J., 2014. A comparison of two-fluid model, dense discrete particle model and CFD-DEM method for modeling impinging gas–solid flows. *Powder Technol.* 254, 94–102.
- Cornelissen, J.T., Taghipour, F., Escudie, R., Ellis, N., Grace, J.R., 2007. CFD modelling of a liquid–solid fluidized bed. *Chem. Eng. Sci.* 62, 6334–6348.
- Deb, S., Tafti, D.K., 2014. Two and three dimensional modeling of fluidized bed with multiple jets in a DEM-CFD framework. *Particology* 16, 19–28.
- Ding, J., Gidaspow, D., 1990. A bubbling fluidization model using kinetic theory of granular flow. *AIChE J.* 36 (4), 523–538.
- Escudero, D.R., Heindel, T.J., 2014. Acoustic fluidized bed hydrodynamics characterization using X-ray computed tomography. *Chem. Eng. J.* 243, 411–420.
- Fede, P., Simonin, O., Ingram, A., 2016. 3D numerical simulation of a lab-scale pressurized dense fluidized bed focussing on the effect of the particle–particle restitution coefficient and particle–wall boundary conditions. *Chem. Eng. Sci.* 142, 215–235.
- Gidaspow, D., 1994. Multiphase Flow and Fluidization. Academic Press.
- Gobin, A., Neau, H., Simonin, O., Llinas, J., Reiling, V., Selo, J., 2001. Numerical simulations of a gas-phase polymerization reactor. In: Proceedings of European Congress on Computational Methods in Applied Sciences and Engineering, Wales.
- Golriz, M.R., Grace, J.R., 2002. Augmentation of heat transfer by deflectors on circulating fluidized bed membrane walls. *Int. J. Heat Mass Transfer* 45, 1149–1154.
- Golshan, S., Zarghami, R., Mostoufi, N., 2017. Hydrodynamics of slot-rectangular spouted beds: process intensification. *Chem. Eng. Res. Des.* 121, 315–328.
- Grace, J.R., Avidan, A.A., Knowlton, T.M., 1997. Circulating Fluidized Beds. Blackie Academic and Professional.
- Grace, J.R., Sun, G., 1991. Influence of particle size distribution on the performance of fluidized bed reactors. *Can. J. Chem. Eng.* 69, 1126–1134.
- Gu, Y., Ozel, A., Sundaresan, S., 2016. Numerical studies of the effects of fines on fluidization. *AIChE J.* 62 (7), 2271–2281.
- Guio-Perez, D.C., Hofbauer, H., Proll, T., 2013. Effect of ring-type internals on solids distribution in a dual circulating fluidized bed system — cold flow model study. *AIChE J.* 59 (10), 3612–3623.
- Guio-Perez, D.C., Proll, T., Hofbauer, H., 2014. Influence of ring-type internals on the solids residence time distribution in the fuel reactor of a dual circulating fluidized bed system for chemical looping combustion. *Chem. Eng. Res. Design* 92, 1107–1118.
- Gunn, D.J., 1978. Transfer of heat or mass to particles in fixed and fluidized beds. *Int. J. Heat Mass Transfer* 21, 467–476.
- Gupta, P., Sun, J., Ooi, J.Y., 2016. DEM-CFD simulation of a dense fluidized bed: wall boundary and particle size effects. *Powder Technol.* 293, 37–47.
- Heindel, T.J., Gray, J.N., Jensen, T.C., 2008. An X-ray system for visualizing fluid flows. *Flow Meas. Instrum.* 19, 67–78.
- Jiang, P., Bi, H., Jean, R.H., Fan, L.-S., 1991. Baffle effects on performance of catalytic circulating fluidized bed reactor. *AIChE J.* 37, 1392–1400.
- Jin, H., Yang, S., Guo, Z., Guangxiang, H., Tong, Z., 2005. The axial distribution of holdups in an industrial-scale bubble column with evaluated pressure using gamma ray attenuation approach. *Chem. Eng. J.* 115, 45–50.
- Khoe, G.K., Ip, T.L., Grace, J.R., 1991. Rheological and fluidization behavior of powders of different particle size distribution. *Powder Technol.* 66, 127–141.
- Kingston, T.A., Geick, T.A., Robinson, T.R., Heindel, T.J., 2015. Characterizing 3D granular flow structures in a double screw mixer using X-ray particle tracking velocimetry. *Powder Technol.* 278, 211–222.
- Klenov, O.P., Noskov, A.S., Parahin, O.A., 2017. Investigation of behaviors of the circulating fluidized bed. *Chem. Eng. J.* 329, 66–76.
- Kono, H.O., Chiba, S., Ells, T., Suzuki, M., 1986. Characterization of the emulsion phase in fine particle fluidized beds. *Powder Technol.* 48, 51–58.
- Kono, H.O., Ells, T.S., Chiba, S., Suzuki, M., Morimoto, E., 1987. Quantitative criteria for emulsion phase characterization and for the transition between particulate and bubbling fluidization. *Powder Technol.* 52, 69–76.
- Kunii, D., Levenspiel, O., 1991. Fluidization Engineering. Butterworth-Heinemann.
- Li, T., Benyahia, S., 2013. Evaluation of wall boundary condition parameters for gas–solids fluidized bed simulations. *AIChE J.* 59 (10), 3624–3632.

- Liu, Y., Hinrichsen, O., 2014a. CFD modeling of bubbling fluidized beds using OpenFOAM: model validation and comparison of TVD differencing schemes. *Comput. Chem. Eng.* 69, 75–88.
- Liu, Y., Hinrichsen, O., 2014b. Study on CFD-PBM turbulence closures based on $k-\varepsilon$ and Reynolds stress model for heterogeneous bubble column flows. *Comput. Fluids* 105, 91–100.
- Loha, C., Chattopadhyay, H., Chatterjee, P.K., 2013. Euler–Euler CFD modeling of fluidized bed: influence of specularity coefficient on hydrodynamic behavior. *Particuology* 11, 673–680.
- Lun, C.K.K., Savage, S.B., Jeffrey, D.J., 1984. Kinetic theories for granular flow: inelastic particles in couette flow and slightly inelastic particles in a general flow field. *J. Fluid Mech.* 140, 223–256.
- Mandal, D., Sharma, V.K., Pant, H.J., Sathiyamoorthy, D., Vinjamur, M., 2012. Quality of fluidization in gas–solid unary and packed fluidized beds: an experimental study using gamma ray transmission technique. *Powder Technol.* 226, 91–98.
- Marschall, H., Mornhinweg, R., Kossmann, A., Oberhauser, S., Langbein, K., Hinrichsen, O., 2011. Numerical simulation of dispersed gas/liquid flows in bubble columns at high phase fractions using OpenFOAM: part II — numerical simulations and results. *Chem. Eng. Technol.* 34 (8), 1321–1327.
- Movahedirad, S., Dehkordi, A., Banaei, M., Deen, N.G., van Sint Annaland, M., Kuipers, J.A.M., 2012. Bubble size distribution in two-dimensional gas–solid fluidized beds. *Ind. Eng. Chem. Res.* 51 (18), 6571–6579.
- Movahedirad, S., Dehkordi, A.M., Molaei, E.A., Hagh, M., Banaei, M., Kuipers, J.A.M., 2014. Bubble splitting in a pseudo-2D gas–solid fluidized bed for Geldart B-type particles. *Chem. Eng. Technol.* 37 (12), 2096–2102.
- Nosrati, K., Movahedirad, S., Sobati, M.A., 2018. Pressure wave attenuation in a gas solid fluidized bed: effects of particles size, density and the electrostatic charge. *Powder Technol.* 236, 281–287.
- Ogawa, S., Umemura, A., Oshima, N., 1980. On the equation of fully fluidized granular materials. *J. Appl. Math. Phys.* 31, 483–493.
- van Ommen, J.R., Nijenhuis, J., van den Bleek, C.M., Coppens, M., 2007. Four ways to introduce structure in fluidized bed reactors. *Ind. Eng. Chem. Res.* 46, 4236–4244.
- Patel, A.K., Waje, S.S., Thorat, B.N., Mujumdar, A.S., 2008. Tomographic diagnosis of gas maldistribution in gas–solid fluidized beds. *Powder Technol.* 185, 239–250.
- Peng, G., Dong, P., Li, Z., Wang, J., Lin, W., 2013. Eulerian simulation of gas–solid flow in a countercurrent downer. *Chem. Eng. J.* 230, 406–414.
- Piovano, S., Salierno, G.L., Montmany, E., D'Agostino, M., Maestri, M., Cassanello, M., 2015. Bed expansion and particle classification in liquid fluidized beds with structured internals. *Chem. Eng. Technol.* 38 (3), 423–430.
- Rossbach, V., Utzig, J., Decker, R.K., Noriler, D., Meier, H.F., 2016. Numerical gas–solid flow analysis of ring-baffled risers. *Powder Technol.* 297, 320–329.
- Saayman, J., Ellis, N., Nicol, W., 2013. Fluidization of high-density particles: the influence of fines on reactor performance. *Powder Technol.* 245, 48–55.
- Sadegheigi, R., 2012. *Fluid Catalytic Cracking Handbook*. Butterwort-Heinemann.
- Samruamphianskun, T., Piumsomboon, P., Chalermsinsuwan, B., 2012. Effect of ring baffle configurations in a circulating fluidized bed riser using CFD simulation and experimental design analysis. *Chem. Eng. J.* 210, 237–251.
- Shuai, W., Tianyu, Z., Guodong, L., Huilin, L., Liyan, S., 2015. Multi-scale heat transfer in fluidized bed reactors by Eulerian CFD modeling. *Fuel* 139, 646–651.
- Solov'ev, S.A., Egorov, A.G., Lamberov, A.A., Egorova, S.R., Kataev, A.N., 2016. Effect of the design of a feedstock injection device in a fluidized bed reactor on the efficiency of the reaction, using the dehydrogenation of iso-paraffins in a fluidized chromia-alumina catalyst bed as an example. *Catal. Ind.* 8 (1), 48–55.
- Syamlal, M., 1987. The Particle-Particle Drag Term in a Multiparticle Model of Fluidization. EG & G Washington Analytical Service Center.
- Upadhyay, M., Park, J.-H., 2015. CFD simulation via conventional two-fluid model of a circulating fluidized bed riser: influence of models and model parameters on hydrodynamic behavior. *Powder Technol.* 272, 260–268.
- Wang, F., Marashdeh, Q., Wang, A., Fan, L.-S., 2012. Electrical capacitance volume tomography imaging of three-dimensional flow structures and solids concentration distributions in a riser and a bend of a gas–solid circulating fluidized bed. *Ind. Eng. Chem. Res.* 51 (33), 10968–10976.
- Wang, X.S., Rhodes, M.J., 2005. A DEM study of particle motion near the walls of gas fluidized beds. *Powder Technol.* 160, 15–19.
- Yang, S., Li, H., Zhu, Q., 2015. Experimental study and numerical simulation of baffled bubbling fluidized beds with Geldart A particles in three dimensions. *Chem. Eng. J.* 259, 338–347.
- Yang, S., Peng, L., Liua, W., Zhao, H., Lv, X., Li, H., Zhu, Q., 2016. Simulation of hydrodynamics in gas–solid bubbling fluidized bed with louver baffles in three dimensions. *Powder Technol.* 296, 37–44.
- Yang, W.C., 2003. *Handbook of Fluidization and Fluid-Particle System*. Taylor and Francis Group.
- Yates, J.G., Newton, D., 1986. Fine particle effects in a fluidized-bed reactor. *Chem. Eng. Sci.* 41, 801–806.
- Zhang, M., Qian, Z., Yu, H., Wei, F., 2003. The near wall dense ring in a large-scale down-flow circulating fluidized bed. *Chem. Eng. J.* 92, 161–167.
- Zhong, H., Gao, J., Xu, C., Lan, X., 2012. CFD modeling the hydrodynamics of binary particle mixtures in bubbling fluidized beds: effect of wall boundary condition. *Powder Technol.* 230, 232–240.
- Zhou, E., Zhao, Y., Duan, C., Yang, X., Yu, X., Li, G., Liufeng, Y., Fan, X., Zhang, Y., 2016. Fluidization characteristics and fine coal dry beneficiation using a pronaion-grille baffle dense phase medium fluidized bed. *Fuel* 185, 555–564.
- Zhou, Q., Wang, C., Wang, H., Wang, J., 2016. Eulerian-Lagrangian study of dense liquid–solid flow in an industrial-scale cylindrical hydrocyclone. *Int. J. Miner. Process.* 151, 40–50.